Surface inspection of joint areas by means of laser-induced breakdown spectroscopy

IOP Conf. Series: Materials Science and Engineering 480 (2019) 012006 doi:10.1088/1757-899X/480/1/012006

Surface inspection of joint areas by means of laser-induced breakdown spectroscopy

P Doraciak[1,*], A Bünting[1] and T Lampke[2]

[1] Process Development, Daimler AG, 70546 Stuttgart, Germany
[2] Institute of Materials Science and Engineering, Chemnitz University of Technology, 09125 Chemnitz, Germany

[*] e-mail: patrik.doraciak@daimler.com

Abstract. The quality of laser welded joints is dependent on different factors like the process-parameters, weld configuration and the cleanliness of the joint area. Filmic contaminations on the joint area can be oil, grease and other lubricants, which are used for machining, corrosion protection or component assembly. Residuals of lubricants can vaporize during the laser welding process and may lead to weld smoke as well as spatters and results in welding defects like cracks and pores in the weld seam. Laser-induced breakdown spectroscopy (LIBS) was investigated successfully and applied to detect contaminants and finally avoid these welding defects. 1.7131 steel was used as model-substrate. The ground sample surfaces were characterized by means of surface energy as well as fluorescence-intensity and LIBS spectra of the cleaned surfaces were recorded. The effect of the laser pulse energy and the delay time between laser pulse and the spectra recording was investigated. Furthermore, a forming lubricant was applied on the sample surfaces and reflectometry was successfully used for the film thickness measurements. LIBS spectra of the contaminated surfaces are presented and the impacts of the oil film thickness on the appearance of the spectra are outlined. Additionally, the examination presents the evaluation of the spectra with the linear correlation and the peak intensity ratio.

1. Introduction

The condition of joint areas in terms of filmic contaminations has a major impact on the quality of laser welded joints [1-3]. Technical products, which are processed by laser welding, are usually treated beforehand by various machining processes. Residuals of oil, grease and other lubricants from metal forming, milling, drilling and other machine processing can be found on the surfaces. Additionally, residuals from chemical cleaning, corrosion protection and the assembly remain on the surfaces. These filmic contaminations can lead to weld smoke, spatters and the ejection of melted material during the welding process as well as defects in the welded joint like cracks and pores [4-6]. Current strategies to ensure an adequate high weld seam quality are adjusted on the application and reach from prior chemical cleaning as well as laser cleaning up to 100 % end of line ultrasonic tests of the weld seams.

Technical regulations demand cleaned surfaces without filmic contaminations such as oil, grease and other lubricants in general to avoid these welding defects [1, 2, 7, 8]. However, a limited selection of measurement methods is available for the detection of organic or carbon-based contaminations on surfaces. Most of them are intended for laboratory use or the composition of the contaminations have to be known sufficiently [9, 10]. Usually, these requirements aren't given. For this reason, the

dependable usage isn't possible or the measurement methods aren't suitable for the industrial inline usage [9-11].

Laser-induced breakdown spectroscopy (LIBS) is a well-known atom emission spectroscopy based measurement technique. The measurement method is used in industrial applications from production control in the steel industry through to the fast classification of metals in the scrap metal sorting by now [12, 13]. LIBS is also used as a tool for surface analysis [14-16] in diverse applications. Especially, [11] used LIBS with a high-resolution echelle spectrometer for the detection of surface contaminations on CFK surfaces and [17] used LIBS with a low resolution spectrometer for the process control of a laser ablation process. Summarized, the LIBS measurement technique is a promising approach for the detection of filmic contaminations on metallic surfaces, suitable for industrial inline use.

The presented study examines the possibility to detect contaminations on surfaces with the laser-induced breakdown spectroscopy. Therefore, a processing routine for samples with a constant and reproducible cleanliness condition as well as cleanliness condition characterization methods are investigated. Additionally, LIBS spectra of cleaned and coated samples are recorded and the possibilities for the contamination detection are examined.

2. Experimental and materials

In context of this study, the case hardening steel 16MnCr5 (1.7131) was used as a model substrate. 16MnCr5 offers good mechanical properties and is a typically used material in the automotive field for powertrain components. The composition of 16MnCr5 is shown in table 1.

Table 1. Composition of 16MnCr5 (1.7131) in wt.-%.

	C	Mn	Cr	Si	S	P
16MnCr5	0.14 to 0.19	1.0 to 1.3	0.8 to 1.1	≤ 0.4	≤ 0.035	≤ 0.035

Every single sample was cut from metal sheets and had the dimensions of V = (70 x 30 x 5) mm³. The samples were ground with a grinding machine Saphir 350 / Rubin 520 from ATM GmbH (Mammelzen, Germany) and a special sample holder. In order to obtain a polished and reflective surface, SiC papers with grit sizes up to 2500 were used. For the surface roughness measurements, the profile method according to DIN EN ISO 4287 was used on three samples with eight single measurements on each sample to get average R_z and R_a roughness values. Figure 1b) depicts sketches of the samples with the measurement positions and directions of the surface roughness measurements (see black arrows).

Every sample was cleaned in a multi-stage cleaning procedure to get a consistent surface cleanliness condition. The entire cleaning routine is shown in figure 2. The samples were hand cleaned with demineralized water after the grinding process to remove abrasive particles. Afterwards, the samples were cleaned in an ultrasonic cleaning process for t = 15 min and T = 30 °C in a mixture of Green Star BMP from Koch-Chemie GmbH (Unna, Germany) and demineralized water at a ratio of 1:20. To remove surfactants from the ultrasonic cleaning, the samples were rinsed with demineralized water and dried with compressed air subsequently. Furthermore, the samples were cleaned with ethyl alcohol, 2-propanol and petroleum benzine for t = 5 min in each case. The used solvents are suitable for analytical use. After each solvent bath the samples were dried with compressed air.

Two different methods were applied for the cleanliness condition characterization of the samples. In the first step, the average surface energies were determined for six samples. For this purpose an OCA 25 contact angle measurement device of DataPhysics Instrument GmbH (Filderstadt, Germany) was used. It is offering an automatically drop application, a visualization of the drops and a calculation of the contact angles. Contact angles were recorded at three different positions on each sample as shown in figure 1c) and the surface energy σ was calculated. As test liquids demineralized water, diiodomethane, ethylene glycol and thiodiglycol were used because of their different polar and

disperse shares. The calculation of the surface energy was performed with the method from Owens, Wendt, Rabel & Kälble (OWRK) [18-20].

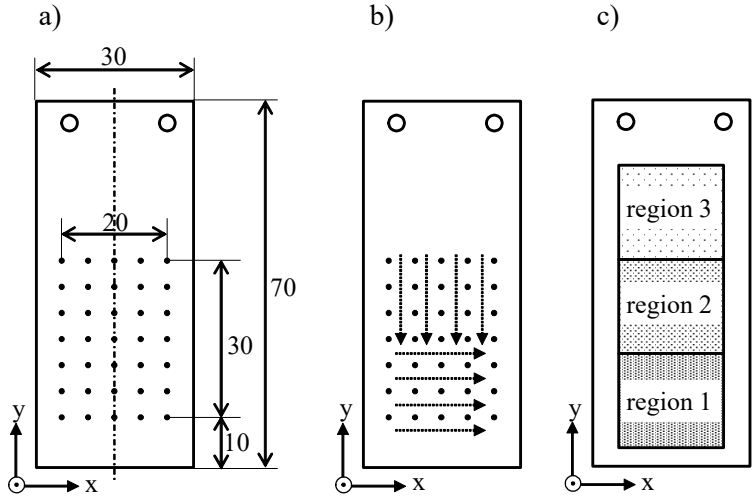

Figure 1. Sketches of the samples. a) Dimension of the samples with the position and the size of the measurement field for fluorescence measurements, LIBS measurements and film thickness measurements. b) Positions and directions of the surface roughness measurements. c) Positions of the three regions for the surface energy measurements.

The fluorescence intensity of the sample surfaces were measured as second method for the cleanliness condition characterization. For this purpose, the F-Scanner from Fraunhofer ipm (Freiburg, Germany) was used. The F-Scanner is a device to detect laser-induced fluorescence emitted from organic or carbon-based contaminations on surfaces. Therefore, the sample surface is inspected with a semiconductor laser operating at a wavelength of $\lambda = 405$ nm. Thus, contaminations on the surface are excited to fluorescence. The emitted fluorescence is detected in a wavelength range between $\lambda = 420$ nm and $\lambda = 520$ nm. The voltage at the detector U_F or the percentage value of the fluorescence intensity related to the USFS 461 standard is given for every pixel as measurement result [21]. The measurement range is adjustable so that impacts from surface roughness or contaminations, which exhibit different fluorescence intensities, could be compensated. The detector voltage U_F was recorded at 35 positions of every sample for an average fluorescence value as shown in figure 1a).

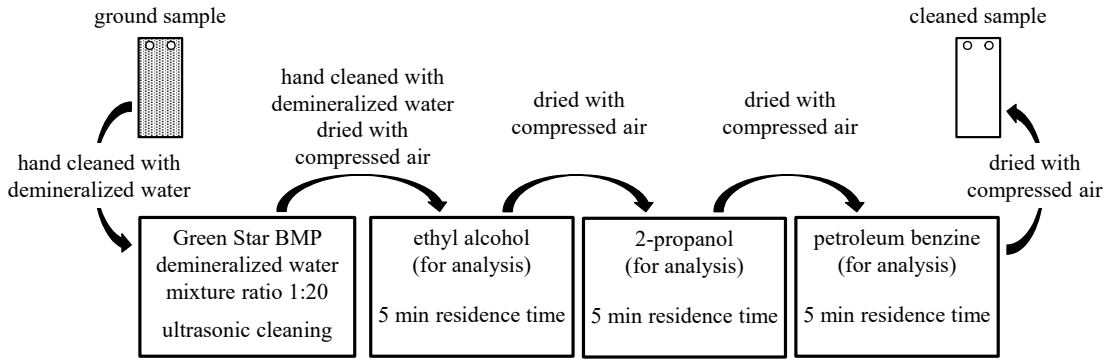

Figure 2. Multi-stage cleaning routine for the ground samples.

For the examination of contaminated surfaces, the forming lubricant Wisura Akalit CF10 from Fuchs Wisura GmbH (Bremen, Germany) was applied on the samples. This forming lubricant is used in

some other investigations as a reference contamination [9, 22]. Varying film thicknesses were achieved by dip-coating with different coating velocities in the range from $v = 100$ mm·min^{-1} to $v = 530$ mm·min^{-1} and variable lubricant solvents mixtures [23, 24]. The film thickness was measured with a reflectometry measurement system. Reflectometry is normally used for layer thickness measurements in the semiconductor industry but can also be used for the measurement of transparent oil films. Polychromatic light is directed perpendicularly to the surface and is partially reflected at the interface between the ambient air and the oil film. The other part of the light is transmitted and finally reflected at the interface between the oil film and the substrate. The two reflected light beams interfere due to the optical path difference. The interfered light beam is coupled into an optical fiber and the interference pattern, which is mainly depending on the film thickness, is recorded by a fiber-coupled spectrometer. With the knowledge of the optical properties of the substrate and the oil, the film thickness can be calculated with a computer software. The oil film thickness was measured according to figure 1a) at 35 positions (see black dots) on the sample to achieve an average value of the film thickness.

Laser-induced breakdown spectroscopy is a method for the detection of chemical elements and belongs to the group of atom emission spectroscopy. The method is widely described in [25, 26] as well as [27] and used for research and industrial applications. For this study a standard laboratory setup was used as illustrated in figure 3. The pulsed laser radiation for the plasma ignition is provided by a flash lamp pumped Q-switched Nd:YAG laser (Q-Smart 450, Quantel Laser, Les Ulis Cedex, France) operating at a wavelength of $\lambda = 1064$ nm with a pulse repetition rate of $f_{rep} = 10$ Hz. The pulse duration is fixed at $t_p = 6$ ns (FWHM). The laser beam was focused onto the surface with a plano-convex lens with a focal length of $f = 200$ mm and an anti-reflection coating for $\lambda = 532$ nm and $\lambda = 1064$ nm. The plasma emission was coupled out by a dichroic mirror with an average reflection $R > 95$ % in a wavelength range of 420 nm $\leq \lambda \leq$ 900 nm. The plasma emission was observed by the fiber coupled czerny-turner spectrometer HR2000+ from OceanOptics Inc. with a 25 µm entrance slit and a grit with 600 grooves mm^{-1}, centered on $\lambda = 500$ nm. The CCD detector offers 2048 pixels and a resulting spectral recording range of 393 nm $\leq \lambda \leq$ 845 nm at a resolution of $\Delta\lambda = 0.22$ nm. The shortest integration time of the CCD is $t_I = 1$ ms.

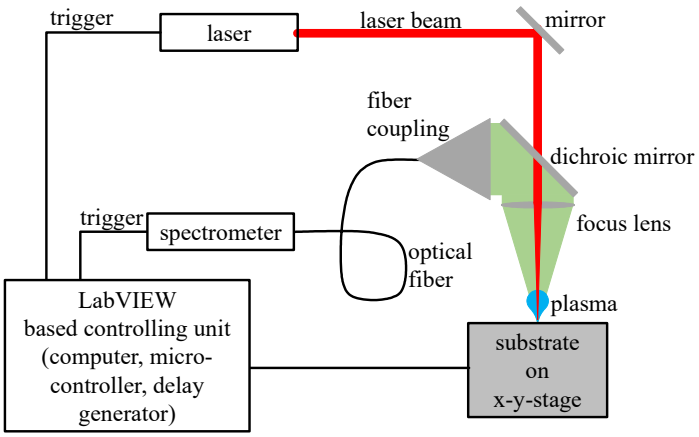

Figure 3. Standard LIBS measurement setup for laboratory use [25].

The measurement system is equipped with two linear stages from Physik Instrumente (PI) (Karlsruhe, Germany) offering an x-y-measurement range of $A = (180 \times 180)$ mm². The stages as well as the laser and spectrometer are controlled by a self-developed software tool based on LabVIEW and a microcontroller type chipKIT Max32 from Digilent Inc (Pullman, USA). The LabVIEW software tool sets the program for the linear stages. The microcontroller triggers two delay generators (AFG3051C

and AFG3022B, Tektronix GmbH, Köln, Germany), which supply trigger signals for the laser flash lamp, laser Q-switch and the spectrometer. The duration between the firing of the laser pulse and the start of the integration time is defined as delay time t_d. The recorded spectra are saved on the computer for the evaluation process.

Two different ways for the evaluation of the spectral data are investigated. The linear correlation coefficient r, with

$$r = \frac{\sum_{i=1}^{m}\left(x_i - \overline{x}\right)\left(y_i - \overline{y}\right)}{\left[\sum_{i=1}^{m}\left(x_i - \overline{x}\right)^2\right]^{1/2}\left[\sum_{i=1}^{m}\left(y_i - \overline{y}\right)^2\right]^{1/2}} \quad (1),$$

is a calculated value for the relationship of two data sets. It ranges from -1 to 1 at which $r = 1$ means a 100 % positive correlation, $r = -1$ means a 100 % negative correlation and $r = 0$ means no correlation. The linear correlation coefficient r is invariant against linear variations. It means that an overall offset or a factorization of the data set doesn't influence the correlation coefficient r [28].

Hence, it's used for the evaluation of spectral data in many other LIBS applications like the sample identification or the recognition of solid layers [17, 28]. Usually, a set of measured spectra are linearly correlated with a reference spectrum. The calculation of the reference spectrum is described in equation (2). A set of S_i to S_n spectra is given in which n is the number of recorded spectra, $i \in (1,...n)$ Every single spectrum S_i has a set of 2048 intensity values $I_{i,\,P1}$ to $I_{i,\,P2048}$. With this data, the reference spectrum can be calculated by

$$S_{\mathrm{Ref}} = \begin{pmatrix} \frac{1}{n}\sum_{i=1}^{n} I_{i,\mathrm{P1}} \\ \vdots \\ \frac{1}{n}\sum_{i=1}^{n} I_{i,\mathrm{P2048}} \end{pmatrix}. \quad (2)$$

A further method for the investigation of LIBS spectra is the calculation of the peak intensity ratio k [25]. Two peak intensities from different elements are used. This technique is often applied with calibration curves for the determination of element concentrations in materials. For the investigation of coating thicknesses, two different element lines are necessary. The first element line occurs typically in the spectrum of the substrate (without coating) and is used as a reference line. The second element line is characteristic for the coating and occurs in the spectrum of the coating. If the thickness of the coating increases, the emission intensity of the second line increases, too, because of the higher element occurrence in the ablated material. The emission intensity of the first line decreases concurrently and the intensity ratio of the two element lines increases [11, 12, 29]. The calculation of the peak intensity ratio k is given by the equation

$$k = \frac{I_{\lambda_2}}{I_{\lambda_1}}. \quad (3)$$

3. Results and discussion

First of all, the surface roughness of the ground samples was measured. The cleanliness condition of the cleaned surfaces was investigated with the measurement of the surface energy and the laser-induced fluorescence. LIBS spectra of the cleaned surface were recorded and the impact of laser pulse energy and delay time determined. Additionally, occurred element lines were determined. In the

second part of the study, samples with applied oil films were investigated. The film thickness was measured with reflectometry and the LIBS measurement of the equal samples were carried out.

3.1. Characterization of cleaned sample surfaces

The surface roughness measurement was performed using the profile method for x- and y-direction. Three samples with four single measurements for both directions on each sample were executed and the average R_z and R_a values were calculated. The results of the measurements are shown in table 2. The average R_z values amount between 0.12 ± 0.01 µm and 0.13 ± 0.02 µm in x- and y-direction. The average R_a values amount between 0.016 ± 0.001 µm and 0.018 ± 0.002 µm, as well in both directions. All single average R_z and R_a values exhibit only marginal standard deviations in the range of $0.01\ \mu m \leq s_{Rz} \leq 0.02\ \mu m$ and $0.001\ \mu m \leq s_{Ra} \leq 0.003\ \mu m$. As expected, the samples exhibit a nearly constant and reproducible surface roughness without significant differences in x- and y-direction. This can be explained by the well-defined and automated grinding process.

Table 2. Surface roughness R_z and R_a of the samples in x- and y-direction.

	x-direction		y-direction	
Sample No.	R_z / µm	R_a / µm	R_z / µm	R_a / µm
1	0.12 ± 0.01	0.016 ± 0.001	0.12 ± 0.01	0.015 ± 0.001
2	0.13 ± 0.01	0.016 ± 0.001	0.13 ± 0.02	0.017 ± 0.003
3	0.12 ± 0.01	0.016 ± 0.002	0.13 ± 0.01	0.018 ± 0.002

The surface energy was determined at three sites on six samples to get average values of the surface energy as well as disperse and polar shares. Figure 4 shows the results. The average surface energy for all six samples amount $\bar{\sigma} = 46.2 \pm 0.5$ mN/m with $\bar{\sigma}_{Disperse} = 4.9 \pm 0.5$ mN/m and $\bar{\sigma}_{Polar} = 41.3 \pm 0.4$ mN/m. The average surface energy values of the single samples are very consistent and in a range of $\sigma_{min} = 45.7 \pm 0.7$ mN/m and $\sigma_{max} = 47.0 \pm 0.9$ mN/m. The disperse share is between $\sigma_{disperse,\ min} = 4.42 \pm 0.43$ mN/m and $\sigma_{disperse,\ max} = 5.82 \pm 1.35$ mN/m, the polar share is between $\sigma_{polar,\ min} = 41.01 \pm 1.02$ mN/m and $\sigma_{polar,\ max} = 42.12 \pm 0.12$ mN/m.

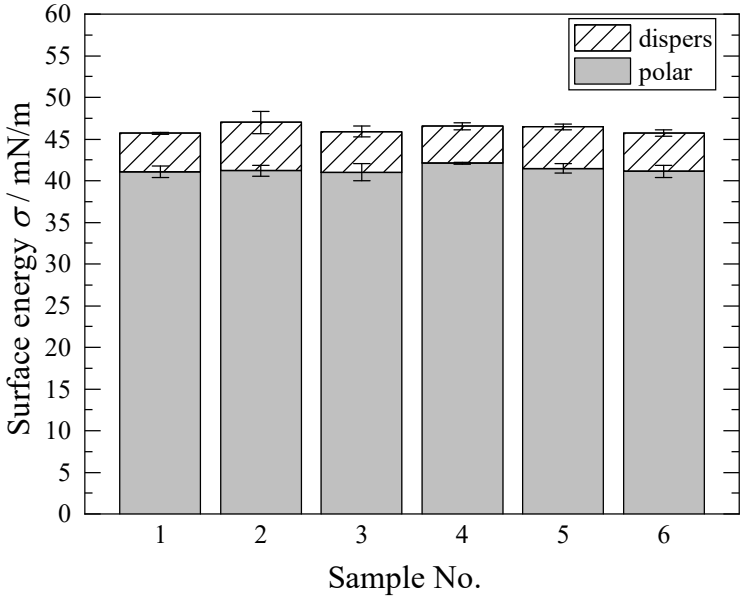

Figure 4. Surface energy of the six measured samples. The disperse and polar shares are illustrated.

The results of the fluorescence measurements for 115 samples are shown in figure 5. Every data point represents the average detector voltage U_F of 35 measurements on the sample. As well as the standard deviation, the 95 % confidence interval is shown for every sample. The average detector voltage for all 115 samples is very low with $\overline{U}_F = 3.21 \cdot 10^{-3} \pm 0.31 \cdot 10^{-3}$ V. Differences in the values appear in the third digit after the decimal point. The minimal und maximum values amount $U_{F,\,min} = 2.15 \cdot 10^{-3} \pm 0.29 \cdot 10^{-3}$ V and $U_{F,\,max} = 4.05 \cdot 10^{-3} \pm 0.83 \cdot 10^{-3}$ V. For comparison, a film thickness d_s of $d_s = 125 \pm 6$ nm of Wisura Akalit CF 10 lead to an average detector voltage of $\overline{U}_F = 266.2 \cdot 10^{-3} \pm 13.8 \cdot 10^{-3}$ V. The results of the fluorescence measurements demonstrate that a constant and reproducible cleanliness condition can be produced.

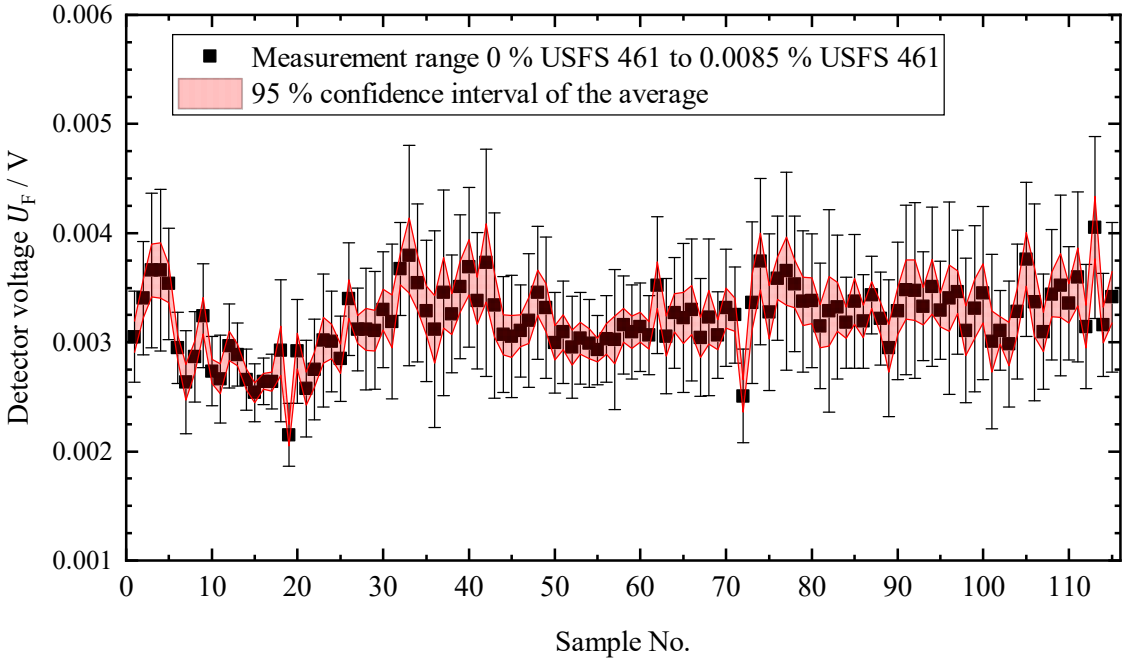

Figure 5. Fluorescence intensity, measured as detector voltage U_F of 115 cleaned samples. The standard deviations as well as the 95 % confidence intervals are shown.

3.2. LIBS measurements of cleaned sample surfaces

The LIBS laboratory setup as shown in figure 3 was used for the LIBS spectra recording of the cleaned samples. The cleaned samples were overall placed at a constant distance to the lens. Different power densities Ψ in the range of 2.07 GW·cm^{-2} to 3.21 GW·cm^{-2} were used to analyze the impact of the laser pulse energy. The delay time between the firing of the laser pulse and the recording of the spectrum was varied from $t_d = 500$ ns to $t_d = 6000$ ns. 35 spectra were recorded for every combination of power density and delay time and the average spectra were calculated.

Figure 6 shows the change of the spectra with increasing delay time for the power density of $\Psi = 2.83$ GW·cm^{-2}. In the time range till $t = 1$ µs after the laser pulse, the strong continuum emission is visible [26]. In the time range of $t = 1$ µs to $t = 3$ µs, spectra with decreasing continuum emission and increasing emission intensity of the discrete element lines can be observed. In the time range $t > 3$ µs, the emission intensity of the element lines decreases fast. This behaviour is also described in basic literature of laser-induced breakdown spectroscopy [26, 27, 30].

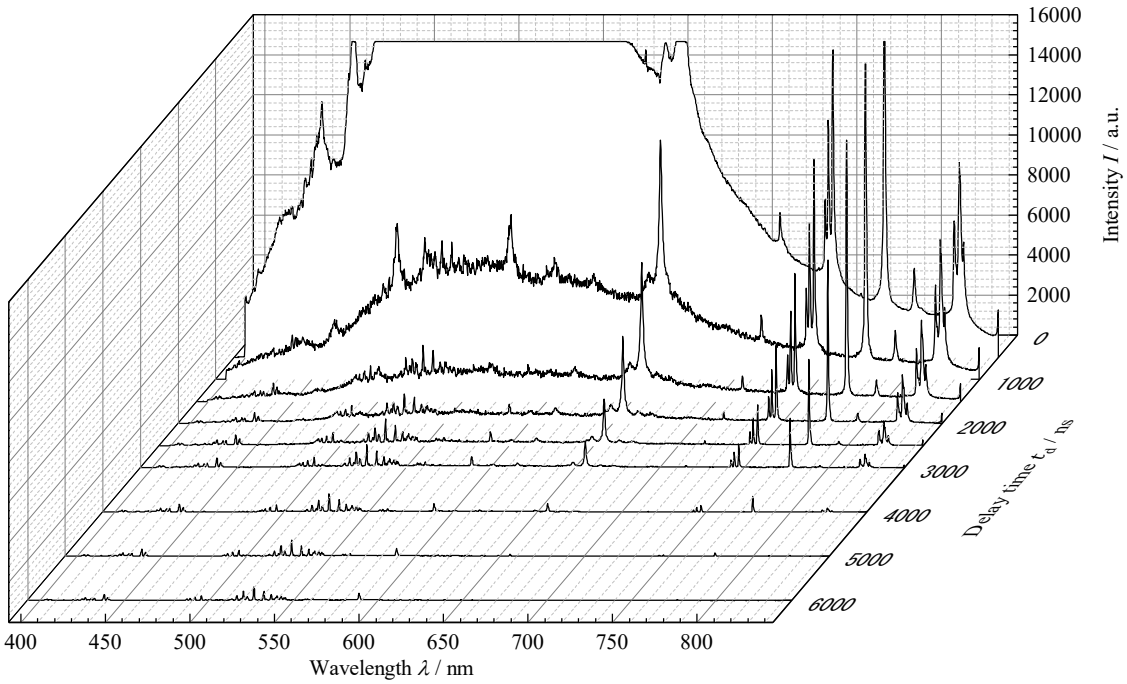

Figure 6. Trend of the spectrum as a function of the delay time for a power density of $\Psi = 2.83$ GW·cm^{-2}.

Figure 7 illustrates the emission intensity $I_{\lambda = 777.27}$ of the oxygen line at $\lambda = 777.27$ nm depending on the power density and the delay time. It is easily visible, that the emission intensity reaches the saturation of the spectrometer for the first 500 ns after the laser pulse is fired. For all power densities, the decrease of the emission intensity shows the same trend, but it is shifted to higher delay times for higher power densities. For the lowest power density, the decrease of the emission intensity starts immediately.

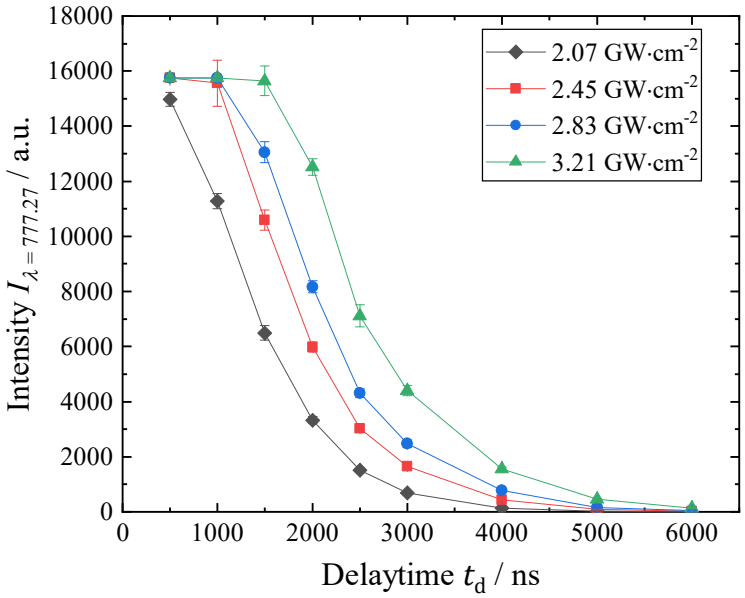

Figure 7. Trend of the emission intensity of the oxygen element line at $\lambda = 777.27$ nm as a function of the delay time t_d and the power density Ψ.

Figure 8 shows the reference spectrum for $\Psi = 2.83$ GW·cm^{-2}. The reference spectrum was calculated from $n = 35$ spectra as described in equation (2). The spectrum exhibits a marginal ratio of continuum emission and the emission of some discrete element lines. It is noticeable that the explicit visible element lines are elements contained in ambient air like oxygen, nitrogen and hydrogen. Element lines from the metallic substrate aren't explicitly visible. There are two possible explanations for this behavior. First, the samples were positioned behind the focal point which means that the laser beam had to pass the focal point of the beam waist. This can favor fail ignitions in the focal point. Fail ignitions occurred rarely and were not reproducible in the performed investigations.

Additional investigations with diffuse surfaces point at a second and more conclusive explanation. The ability for laser radiation to couple into material is dependent on the diffusivity of the surface [31]. There are bad conditions for the laser radiation to be absorbed by the material because of the high reflectivity of the sample surfaces. Thus, only a small amount of the substrate material can be ablated and the share of stimulated elements from ambient air is bigger. It results in a higher emission intensity of these element lines in comparison to the emission intensity of element lines from the substrate material.

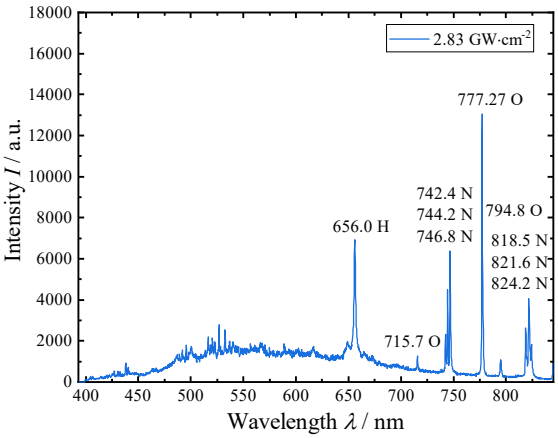

Figure 8. Reference spectrum for $\Psi = 2.83$ GW·cm^{-2} with the identification of the element lines [32].

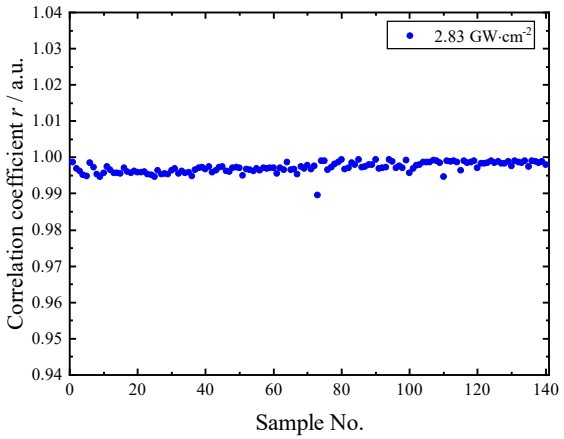

Figure 9. Correlation coefficient r to reference spectrum for 140 single spectra, calculated for $\Psi = 2.83$ GW·cm^{-2}.

Further, reproducibility of the recorded spectra from cleaned sample surfaces was investigated as shown in figure 9. 140 spectra from cleaned sample surfaces were recorded and the correlation coefficients for the linear correlation with the reference spectrum were calculated. Average correlation coefficient amount $\bar{r} = 0.9972 \pm 0.0014$, which relates to a relative standard deviation (RSD) of RSD = 0.144 %. The lower 95 % confidence interval amounts to 0.997, the upper 95 % confidence interval amounts to 0.9975. It is clearly demonstrated for 140 single spectra, that the recorded spectra are reproducible. The results from LIBS measurement of cleaned samples surfaces are conform to the results from the surface energy and fluorescence measurements.

3.3. LIBS measurements of coated sample surfaces

For the investigation of contaminated surfaces, ground and cleaned samples were coated with the forming lubricant Wisura Akalit CF10. The oil film was performed by means of a dip-coating process. Based on the variation of the coating velocity v and the mixture of solvent and lubricant, 19 different film thicknesses d_S were generated. The film thickness d_S was measured using reflectometry at 35 sites on the sample for an average value of the film thickness. LIBS measurements of the coated samples were performed with the laboratory setup as shown in figure 3. On every sample, 35 LIBS

measurements were executed and the average spectra were calculated, analogous to equation 2. All spectra were recorded with power densities in the range of 2.45 GW·cm^{-2} to 3.21 GW·cm^{-2}.

Figure 10 shows five average spectra for $\Psi = 3.21$ GW·cm^{-2} and an increasing film thickness in a range between $d_S \approx 100$ nm and $d_S \approx 3100$ nm. The average spectrum for a film thickness of $d_S \approx 690$ nm is depicted in figure 11. It shows the identified element as well as molecule emission lines for an easier assignability. Taking a look at figure 10, it is obvious that the emission intensity of the visible element lines and molecule emissions change with the film thickness. In the wavelength range between $\lambda = 453.8$ nm and $\lambda = 474.4$ nm C_2 molecule emission [33] increases first and decreases for a film thickness higher than $d_S \approx 750$ nm. The other C_2 molecule emissions between $\lambda = 494.6$ nm and $\lambda = 517.5$ nm, $\lambda = 525.9$ nm and $\lambda = 563.8$ nm as well as between $\lambda = 593.2$ nm and $\lambda = 620.7$ nm show a similar behavior [33]. The hydrogen element line at $\lambda = 656.021$ nm, which was visible in the reference spectrum too, shows an equivalent behavior.

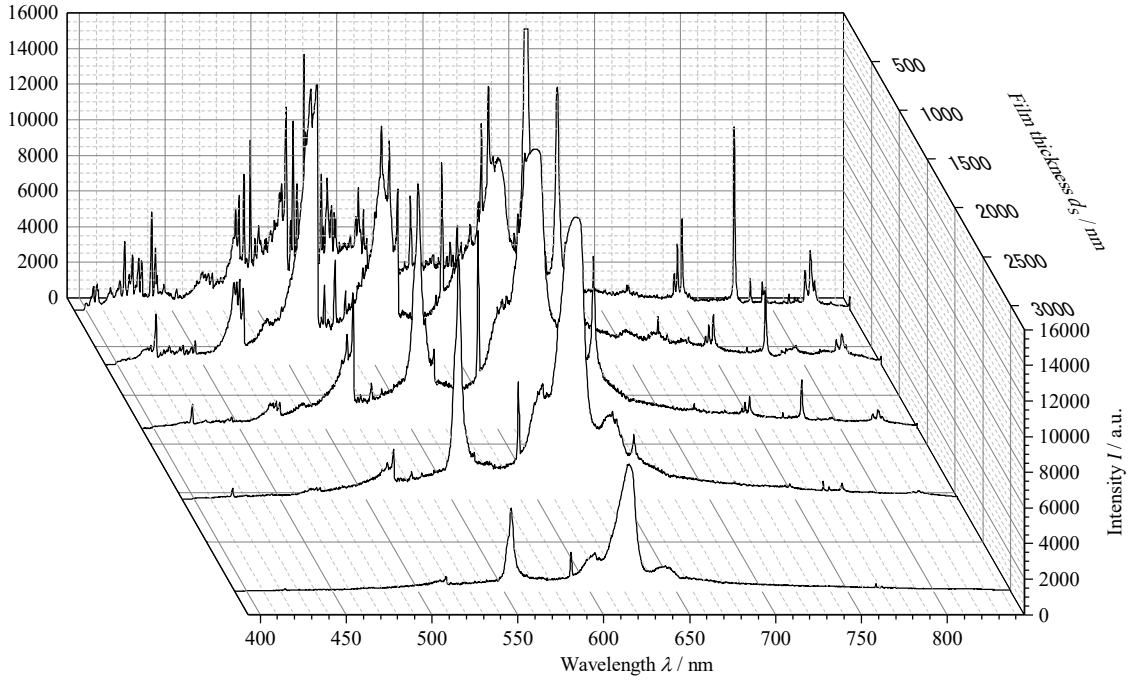

Figure 10. Appearance of the spectrum dependent on film thickness of Wisura Akalit CF 10 for power density $\Psi = 3.21$ GW·cm^{-2}.

The emission intensity of the oxygen element line at $\lambda = 777.27$ nm decreases with increasing film thickness, as shown in figure 12. The decrease in emission intensity is similar for all power densities but it is shifted to higher film thicknesses for higher power densities. Figure 13 shows the evolution of the C_2 molecule emission line at $\lambda = 516.073$ nm (see figure 11). The intensity reaches the saturation of the spectrometer for a film thickness between $d_S \approx 450$ nm and $d_S \approx 700$ nm. For a film thickness $d_S > 700$ nm, the emission intensity decreases. The begin of the decrease in emission intensity is shifted to higher film thicknesses with increasing power density Ψ.

This overall behavior can be explained in the following way: For a marginal film thickness, the power density is high enough to ionize the ablated material. The emission intensity of the C_2 molecule emission increases and the emission intensity of the oxygen element line decreases in this range of film thickness. With increasing film thickness, the power density is no longer high enough to ionize the ablated material completely. The overall intensity of the recorded spectra decreases as shown. The explanation is supported by the shift of the decrease of emission intensity to higher film thicknesses for higher power densities.

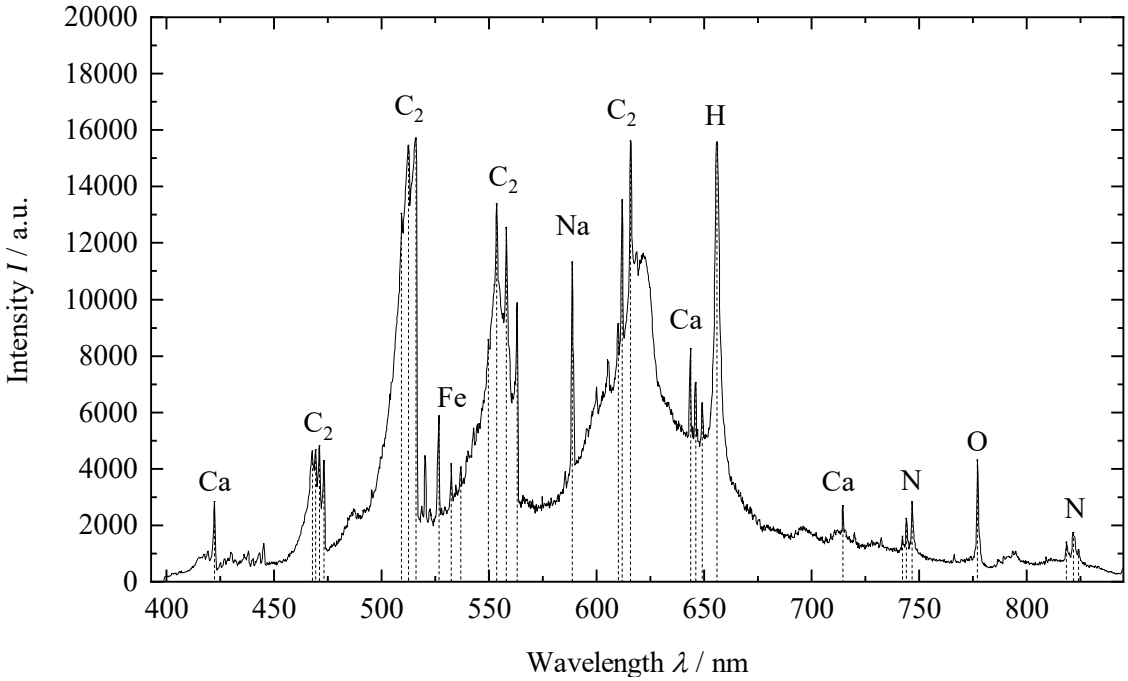

Figure 11. Average spectrum with marked element and molecule emission lines. The film thickness of Wisura Akalit CF 10 amounted $d_s \approx 690$ nm and the power density was $\Psi = 3.21$ GW·cm^{-2}.

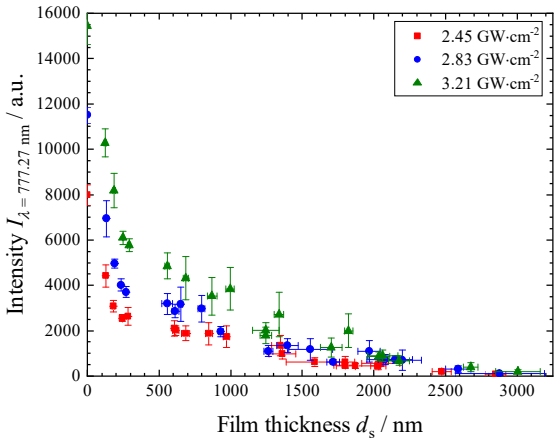

Figure 12. Trend of the emission intensity of the oxygen element line at $\lambda = 777.27$ nm dependent on film thickness d_S of Wisura Akalit CF 10 and power density Ψ.

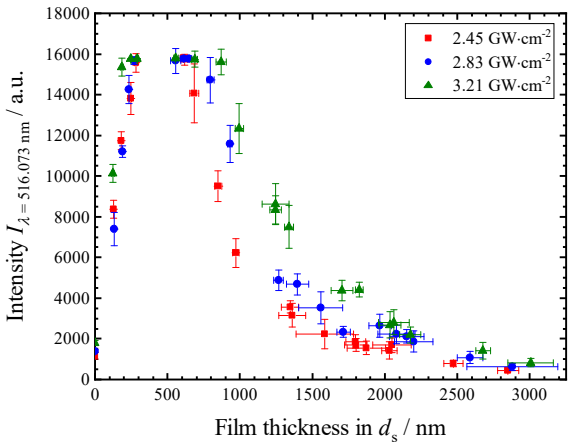

Figure 13. Trend of the emission intensity of the C_2 molecule emission line at $\lambda = 516.073$ nm dependent on film thickness d_S of Wisura Akalit CF 10 and power density Ψ.

The linear correlation coefficient and the peak intensity ratio were used to evaluate the recorded spectra of the coated samples. The principle objective of the investigation is to identify how dependable spectra from coated samples can be distinguished from spectra of cleaned and uncoated samples. For the calculation of the correlation coefficient r, the reference spectra of the cleaned samples were used as a reference data set. The reference spectra of the different power densities were composed as shown in equation (2) from 35 single measurements. Equation (3) was used to calculate the peak intensity ratio. 35 LIBS measurements of every coated sample were recorded and the average correlation coefficient and peak intensity ratio were calculated.

Figure 14 shows the trend of the correlation coefficient r for different power densities dependent on the film thickness. The highest correlation coefficient $r = 0.807 \pm 0.003$ was calculated for a film thickness of $d_S = 57.2 \pm 2.4$ nm at $\Psi = 2.45$ GW·cm^{-2}. In general, the correlation coefficient decreases with increasing film thickness of Wisura Akalit CF10. For thin film thicknesses up to $d_S \approx 450$ nm, the correlation coefficient r decreases nearly linearly with a high gradient. In the range from $d_S \approx 500$ nm to $d_S \approx 1000$ nm, the correlation coefficient stagnates on one level. For a film thickness of $d_S > 1200$ nm, r decreases slowly and approaches a value $r \approx 0.3$. Overall, a higher power density leads to a marginal higher value of the correlation coefficient.

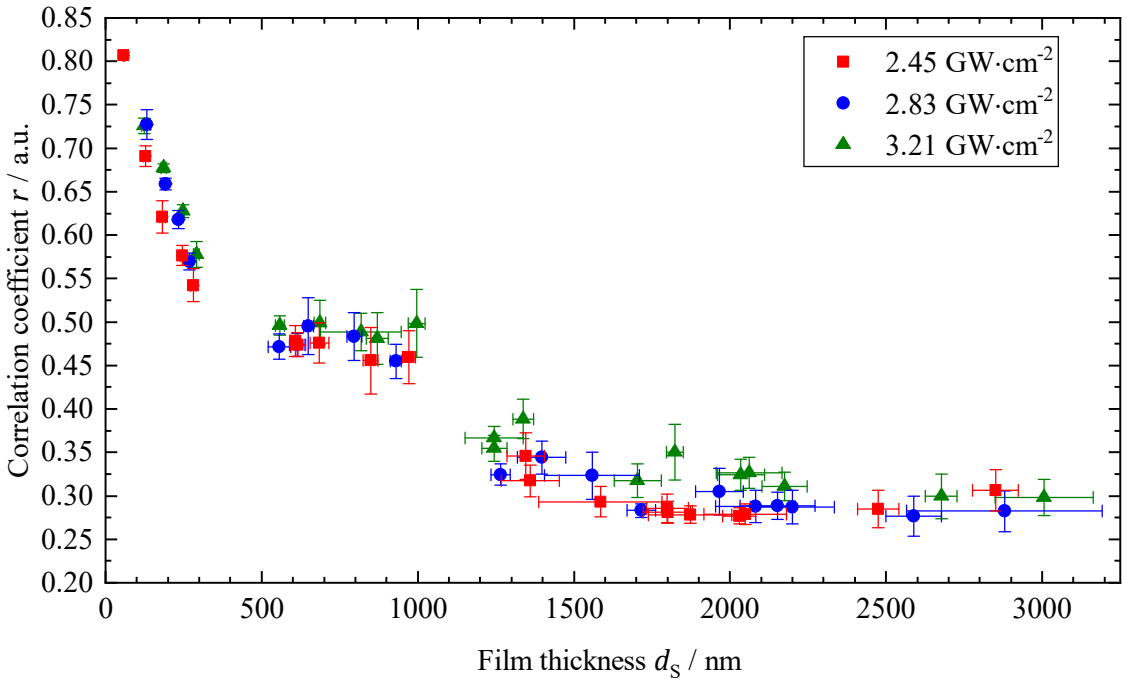

Figure 14. Correlation coefficient r for increasing film thickness and three different power densities.

These three different stages can be explained with the trend of the C_2 molecule emission intensity, shown in figure 13. In the first film thickness region, the element line emission intensities rise rapidly and nearly linearly. Major changes occur in the element line emission intensities and therewith in the data set. In the second region, the element line emission intensity reaches the saturation of the spectrometer detector chip. Additionally, changes in the appearance of the spectra are very marginal. In the third film thickness region, the overall intensity decreases, but the appearance of the spectra changes in a marginal way, see figure 10.

Figure 15 depicts the trend of the peak intensity ratio of the hydrogen line at $\lambda = 656.021$ nm to the oxygen line at $\lambda = 777.27$ nm for the power density $\Psi = 3.21$ GW·cm^{-2}. The peak intensity ratio increases in the film thickness range up to $d_S \approx 600$ nm. Afterwards, the peak intensity ratio approaches to a value of $k \approx 4$ for a film thickness $d_S > 650$ nm. The trend of the peak intensity ratio can be described by a Boltzmann fit. The trend is explained with the course of the intensity of the hydrogen element line and the oxygen element line for increasing film thicknesses, which is depicted in figure 16. The emission intensity of the oxygen element line decreases rapidly in the film thickness region up to $d_S \approx 600$ nm. The emission intensity of the hydrogen element line reaches the saturation of the spectrometer for the same film thickness region. For $d_S > 600$ nm, the oxygen emission intensity and the hydrogen emission intensity decreases steadily with increasing film thickness and a constant peak intensity ratio is reached, see figure 15.

The investigation exhibit, that the linear correlation as well as peak intensity ratio are useable to distinguish spectra of coated samples from spectra of cleaned samples very easily. Additionally, it is shown that the values of the correlation coefficient r and the peak intensity ratio k can't be assigned to film thickness values directly. The correlation coefficient r and the peak intensity ratio k aren't explicit in the examined range of film thicknesses.

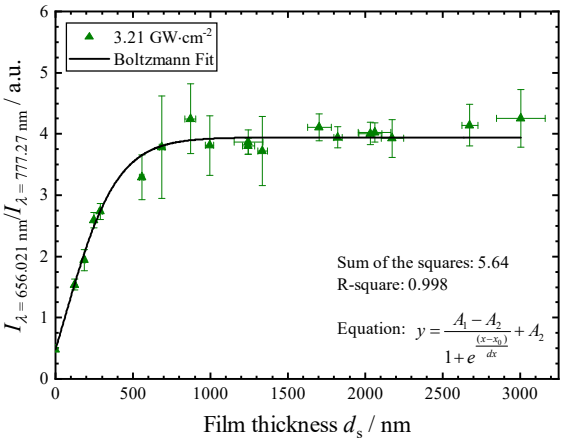

Figure 15. Trend of the peak intensity ratio k of the hydrogen element line at $\lambda = 656.021$ nm to the oxygen element line at $\lambda = 777.27$ nm as a function of the film thickness d_S for the power density $\Psi = 3.21$ GW·cm^{-2}.

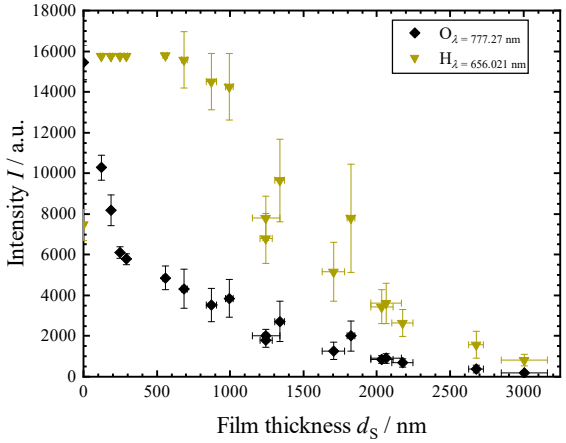

Figure 16. Trend of the emission intensity of the hydrogen element line at $\lambda = 656.021$ nm and the oxygen element line at $\lambda = 777.27$ nm as a function of the film thickness d_S for the power density $\Psi = 3.21$ GW·cm^{-2}.

4. Conclusions

The investigation of the ground samples by means of surface roughness measurements using the profile method showed constant and low surface roughness values without any predominant direction. The examination of the surface energy and the fluorescence detector voltage showed a stable and reproducible cleanliness condition of the samples. The fluorescence detector voltage was measured on 115 samples with 35 measurement points on each sample. The surface energy was measured on three different sites on overall six samples.

The main objective of the investigation was to examine the possibility to locate contaminations on sample surfaces by laser-induced breakdown spectroscopy. In the first step, LIBS measurements were performed on cleaned samples and the impact of the delay time t_d and the power density Ψ were studied. The spectra of the cleaned samples show a strong continuum emission in a short first time range after the laser was fired. The appearance of continuum emission and the time range is well described in [26, 27]. For the next few microseconds, emission of discrete element lines from ambient air occurs. This behavior was also found in another investigation [32]. As expected, the intensity of the element lines decreased with increasing delay time. For increasing power densities, the curve progression looks the same but it is shifted to higher time values. The reference spectra of the cleaned samples were calculated for the examined power densities and correlation coefficients were determined for 140 recorded spectra from cleaned samples. The constant high and reproducible correlation values support the results from the surface energy measurements and the fluorescence measurements.

The samples were coated with Wisura Akalit CF 10 as a model contamination by a dip-coating process. Altogether, 19 different film thickness values were produced and the film thickness was determined using reflectometry. LIBS measurements of the coated sample surfaces were performed with constant delay times and three different power density values. Correlation coefficients in relation to reference spectra of uncoated samples and peak intensity ratios were calculated and investigated.

Summarized, the correlation coefficient *r* shows a decreasing amount with increasing film thickness values. For high film thickness values, the correlation coefficient approximates to a low and nearly constant amount. The peak intensity ratio *k* shows a similar behavior. First, the peak intensity ratio increases with increasing film thickness. Afterwards, the peak intensity ratio approximate to a nearly constant amount for higher film thickness values. The study shows that the linear correlation to reference spectra of cleaned and uncoated samples as well as the peak intensity ratio are suitable to detect lubricant contaminations on sample surfaces. Additionally, both described methods aren't directly suited to determine film thickness values in the investigated film thickness range.

Acknowledgments
The authors acknowledge the Institute of Materials Science and Engineering, Chemnitz University of Technology and the Daimler AG, Stuttgart, for supporting the research. We would also like to thank all colleagues from process development at Daimler AG, above all Mr. Stefan Elischer, for supporting the research.

References
[1] Fahrenwaldt H J and Schuler V 2006 *Praxiswissen Schweißtechnik: Werkstoffe, Prozesse, Fertigung* vol 2 (Wiesbaden: Vieweg)
[2] DVS − Deutscher Verband für Schweißen und verwandte Verfahren e.V. 2015 *Merkblatt DVS 3203-4 Laserstrahlschweißen von metallischen Werkstoffen – Nahtvorbereitung und konstruktive Hinweise* (Düsseldorf: DVS Media)
[3] DVS − Deutscher Verband für Schweißen und verwandte Verfahren e.V. 2009 *Merkblatt DVS 3214 - Unregelmäßigkeiten an Laserstrahlschweißnähten – Ursachen und Abhilfemaßnahmen* (Düsseldorf: DVS Media)
[4] Geiger M, Kägeler C and Schmidt M 2008 High-power laser welding of contaminated steel sheets *Product Engineering - Research and Development* **2** 235–240
[5] Müller M G 2002 *Prozessüberwachung beim Laserstrahlschweißen durch Auswertung der reflektierten Leistung* (München: Herbert Utz)
[6] Wolf M 2006 *Zur Phänomenologie der Heißrissbildung beim Schweißen und Entwicklung aussagekräftiger Prüfverfahren* (Bremerhaven: Wirtschaftsverlag NW)
[7] DVS − Deutscher Verband für Schweißen und verwandte Verfahren e.V. 1993 *Merkblatt DVS 2809 - Laserstrahlschweißen in Elektronik und Feinwerktechnik* (Düsseldorf: DVS Media)
[8] Behler K, Sokolowski W and Beyer E 1987 *Laser Optoelektronik in der Technik: Vorträge des 8. Internationalen Kongresses Laser 87 Optoelektronik* ed Waidelich W (Berlin, Heidelberg: Springer) pp 529-532
[9] Oberhausen M 2007 *Der Einsatz laserinduzierter Fluoreszenzmessungen zur Detektion geringster organischer Belegungen auf Oberflächen* (Saarbrücken: Universität des Saarlandes Produktionstechnik, Dissertation)
[10] Fenske M, Markus S and Hildebrandt H 2012 *Qualitätssicheres Vorbehandeln und Kleben durch den Einsatz optischer Emissionsspektroskopie - Safebond* (Bremen: Forschungsvereinigung Schweißen und verwandte Verfahren)
[11] Markus S 2008 *Die Laser Induced Breakdown Spectroscopy (LIBS) als Inline-Verfahren zur Detektion von Oberflächenkontaminationen im Bereich der Klebtechnik* (Aachen: Shaker)
[12] Noll R, Bette H, Brysch A, Kraushaar M, Mönch I, Peter L and Sturm V 2001 Laser-induced breakdown spectrometry - applications for production control and quality assurance in the steel industry *Spectrochimica Acta Part B* **56** 637–649
[13] Feierabend A 2015 *Recycling und Rohstoffe* vol 8, ed Thomé-Kozmiensky K J and Goldmann D (Neuruppin: TK Verl. Thomé-Kozmiensky) pp 619–628
[14] Vadillo J M and Laserna J J 2004 Laser-induced plasma spectrometry: truly a surface analytical tool *Spectrochimica Acta Part B* **59** 147–161

[15] Vadillo J M, Palanco S, Romero M D and Laserna J J 1996 Applications of laser-induced breakdown spectrometry (LIBS) in surface analysis *Fresenius' Journal of Analytical Chemistry* **355** 909–912
[16] Kratochvíl T, Černohorský T, Knotek P, Kalina L, Návesník J, Pouzara M and Zvolskáa M 2014 Fast determination of the surface density of titanium in ultrathin layers using LIBS spectrometry *Journal of Analytical Atomic Spectrometry* **29** 1806–1812
[17] Lentjes M, Dickmann K and Meijer J 2005 *Aktuelle Methoden der Laser- und Medizinphysik Remagen* ed Hartmann U (Berlin: VDE-Verlag) pp 288–293
[18] Kaelble D H 1970 Dispersion-Polar Surface Tension Properties of Organic Solids *The Journal of Adhesion* **2** 66–81
[19] Owens D K and Wendt R C 1969 Estimation of the surface free energy of polymers *Journal of Applied Polymer Science* **13** 1741–1747
[20] Rabel W 1971 Einige Aspekte der Benetzungstheorie und ihre Anwendung auf die Untersuchung und Veränderung der Oberflächeneigenschaften von Polymeren *Farbe und Lacke* **77** 997–1005
[21] Holz P, Lutz C and Brandenburg A 2017 Optical scanner system for high resolution measurement of lubricant distributions on metal strips based on laser induced fluorescence *Proc. of SPIE* 103292A-1 - 103292A-11
[22] Fischer N 2005 *Messungen geringster organischer Belegungen auf diffus reflektierenden Oberflächen mit einem mIR-faseroptischen Prüfkopf* (Saarbrücken: Universität des Saarlandes Produktionstechnik, Dissertation)
[23] Clint J H 1973 Partial Deposition of Mixed Monolayers onto Solid Surfaces *Journal of Colloid and Interface Science* **43** 132–143
[24] Derjaguin B 1993 On the Thickness of the Liquid Film Adhering to the Walls of a Vessel after Emptying *Progress in Surface Science* **43** 134–137
[25] Noll R 2012 *Laser-Induced Breakdown Spectroscopy: Fundamentals and Applications* vol 1, (Berlin, Heidelberg: Springer)
[26] Miziolek A W Palleschi V and Schechter I 2006 *Laser Induced Breakdown Spectroscopy* vol 1, (Cambridge: Cambridge University Press)
[27] Singh J P and Thakur S N 2007 *Laser-induced breakdown spectroscopy* vol 1, (Amsterdam, Boston, London: Elsevier)
[28] Lentjes M, Dickmann K and Meijer J 2007 Calculation and optimization of sample identification by laser induced breakdown spectroscopy via correlation analysis *Spectrochimica Acta Part B* **62** 56–62
[29] Khater M A 2013 Laser-induced breakdown spectroscopy for light elements detection in steel: State of the art *Spectrochimica Acta Part B* **81** 1–10
[30] Cremers D A and Radziemski L J 2013 *Handbook of laser-induced breakdown spectroscopy* vol 2, (Chichester: John Wiley & Sons)
[31] Hügel H, Dausinger F and Graf T 2007 *Laser in der Fertigung: Strahlquellen, Systeme, Fertigungsverfahren* vol 2 (Wiesbaden: Teubner)
[32] Zhang J 2015 Untersuchungen von laserinduzierten Plasmen in Bohrungen (LIPS) (Mittweida: Hochschule Mittweida, Fakultät Mathematik/Naturwissenschaften/Informatik, Masterthesis)
[33] Lebedev V, Rabchinskii M, Kozlyakov M, Stepanov D, Shvidchenko A, Nikonorov N V and Vul A 2018 Laser-Induced Breakdown Spectroscopy: an advanced method for analysis of nanocarbon materials chemical composition *Journal of Analytical Atomic Spectrometry* **33** 240–250